CANADIAN TUNNELLING CANADIEN

An Annual Publication of
The Tunnelling Association of Canada

Une Publication Annuelle de
L'Association Canadienne des Tunnels

2003

Canadian Tunnelling

Published by

THE TUNNELLING ASSOCIATION OF CANADA

Tunnelling Canadien

Publiée par

L'ASSOCIATION CANADIENNE DES TUNNELS

CANADIAN TUNNELLING CANADIEN publishes papers in English or French concerned with tunnels, shafts, deep excavation or any other aspects of underground construction. Both Canadian and international contributions are welcome.

Manuscripts for publication should be submitted to K.Y. Lo, Department of Civil and Environmental Engineering, Faculty of Engineering, University of Western Ontario, London, Ontario, Canada N6A 5B9.

Printed and bound in Canada

3D ANALYSIS OF STRESSES AROUND AN UNLINED TUNNEL IN ROCK SUBJECTED TO HIGH HORIZONTAL STRESSES

Abdel Meguid, M.
Graduate Student, Department of Civil Engineering, University of Western Ontario, London, ON, Canada

Lo, K. Y.
Director, Geotechnical Research Center, Department of Civil Engineering, University of Western Ontario, London, ON, Canada

Rowe, R. K.
Professor, GeoEngineering Centre at Queen's-RMC, Department of Civil Engineering, Queen's University, Kingston, ON, Canada

ABSTRACT: A 3D elasto-plastic finite element model is used to study the face stability and the corresponding stresses around the face of a tunnel constructed in stress and geological environments prevalent in shales in southern Ontario. The effect of the rock mass strength on the tunnel stability and distribution of stresses at and close to the tunnel face are investigated based on the results of the 3D analyses. The response of the tunnel face to high in-situ horizontal stresses for different rock mass strengths was also examined. To facilitate comparison with plane strain analysis, 3D results are presented for several cross-sections along the tunnel. The potential implications of the results obtained are discussed.

1. INTRODUCTION

When an underground opening is excavated into a stressed rock mass, the stresses in the vicinity of the opening are redistributed such that the tangential stresses are maximum at the periphery of the excavation and decrease with the distance from the tunnel. Therefore, the rock may yield in the overstressed zone surrounding the excavation. Closed form solutions for calculating the stress distribution provide great value for conceptual understanding of behavior and for testing and calibration of numerical models. However, these solutions are restricted to plane strain analysis of simple geometries and material models.

It is known that the ground behavior near the face of an advancing tunnel is a problem that cannot be analyzed by closed form solutions or by simplified plane strain or axisymmetric finite element models because of the strong 3D effects. Several authors have addressed the problem of face stability of tunnels in weak rock. Lo *et al.* [1] presented a theoretical elastic solution for stresses and displacements during the face advance. Lo *et al.* [2] utilized the results of elasto-plastic axisymmetric finite element analysis together with a plane strain closed form solution to introduce the concept of load sharing ratio between the rock mass at the tunnel face and the supporting system. A fictitious support pressure was considered in their analysis by gradually reducing the initial radial stresses inside the tunnel. These studies provided a conceptual framework for interpreting and predicting the displacements, stresses, and stability around the tunnel face.

The objective of this study is to demonstrate some aspects of 3D behavior of large openings in weak rock subjected to high horizontal stresses. A 3D elasto-plastic finite element model is used to study the face stability and the corresponding stresses of a tunnel in Queenston Shale with geometrical and geological conditions similar to those considered for Sir Adam Beck Niagara Generating Station Number 3 (SABNG No. 3) project [3]. Relationships between rock mass strength, circumferential stresses, and plastic zone development at and near the tunnel face are established.

2. ROCK MASS PARAMETERS

The tunnel considered is 13 m diameter and 10 km long located in Queenston Shale at a depth of about 200 m from ground surface. Rock formations in this region are characterized by high initial horizontal stresses. Their magnitudes and directions may vary according to local topographic conditions and geometries.

Based on hydraulic fracturing tests at depth encompassed by most sections of the tunnel, the maximum and minimum horizontal stresses are 24 MPa and 18 MPa respectively. In the analysis, average horizontal stress = 21 MPa, vertical in-situ

stress = 5.2 MPa, and initial stress ratio (K_o) = 4 will be employed.

Reliable estimates of the strength and deformation characteristics of rock mass are required for any analysis involving underground excavation. A representative set of rock parameters used in the analysis is shown in Table 4.1. The uniaxial compressive strength of the rock mass is related to the Mohr-Coulomb parameters by the well known relationship $\sigma_{cm} = (2c \cos\phi) / (1 - \sin\phi)$
where, c and ϕ are the cohesion and angle of internal friction respectively.

Table 1. Rock mass parameters

Rock parameters	
Young's Modulus (E)	15,800 MPa
Poisson's ratio (ν)	0.3
Uniaxial compressive strength:	
- Intact rock (σ_{ci})	37 MPa
- Rock mass (σ_{cm})	37 - 5 MPa
Cohesion (c')	9 – 1.2 MPa
Friction angle (ϕ')	38°
Friction angle (ψ')	0°
Initial stress ratio (K_o)	4
Unit weight (γ)	26 kN/m^3

3. METHOD OF ANALYSIS

The analyses were performed using a three-dimensional (3D) elasto-plastic finite element computer program developed based on the library of routines published by Smith and Griffiths [4] employing the following aspects:

3.1. Full 3D analysis

The rock mass is modeled using 20-noded brick elements. The element performance has been checked against simple cases where closed-form solutions exist for comparison. Details are given elsewhere [5].

3.2. Varied construction sequences

Material is removed at several stages so that, for the non-linear analyses, the final stress data is appropriate to the sequence of excavation that would be performed. This process must be conducted in such a way that equilibrium is maintained in the rock elements around the tunnel. Element removal was carried out using procedure described by Brown and Booker [6]. Initially, the ground is stressed by its own weight. For each excavation stage, the geometry is modified and a new stiffness matrix and load vector is formed. The loads are removed in increments and the nonlinear equations were solved using a modified Newton-Raphson technique. A full integration scheme (27 integration points) was used in the present analysis.

3.3. Material non-linearity

It is assumed that the onset of plastic failure of the rock mass is defined by the Mohr-Coulomb criterion. This failure criterion has an irregular hexagonal shape in principal stress space as shown in Figure 1. The presence of corners at $\theta = \pm 30^o$ creates a non-continuous and non-differentiable failure surface. In the present study, the smoothing algorithm suggested by Smith and Griffiths [4] is adopted, whereby a smooth surface is substituted in the corners when (see Figure 1)

$$| \sin^{-1} \theta | > 0.492424 \ (\theta = 29.5^o).$$

In this region, the surfaces are evaluated explicitly with either $\theta = 30^o$ or $\theta = -30^o$ giving a circular surface over a small arc. Different assumptions can be made, but no numerical difficulties have been encountered with the above scheme.

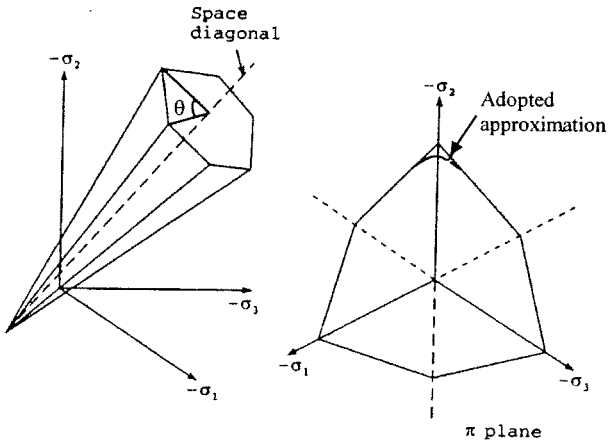

Figure 1. Mohr-Coulomb Failure Criterion in the principal stress space

3.4. Solution algorithm

In a 3D analysis which does not seek to model collapse, reforming and factorizing the global stiffness matrix for the tangent stiffness approach is computationally very costly. Thus for the analyses reported herein, a simple viscoplastic algorithm with a modified Newton-Raphson

iterative scheme is used to redistribute stresses that have strayed outside the failure surface.

3.5. *Pre and post processing*
The graphical interface program GID [7] was used to generate the finite element mesh and to interpret the results of the analysis.

4. ANALYSIS DETAILS

A parametric study was conducted to ensure that the lateral boundaries of the mesh were located sufficiently distant such that they would not significantly influence the predicted displacement of the tunnel lining. To meet this criterion it was necessary to locate the boundaries 88 m (7D) from the tunnel centerline in the x and z-directions. Behind the tunnel face, a distance of 70 m was necessary to ensure that plane strain conditions was reached based on the observed stress and displacement patterns.

The 3D finite element analysis was performed using 1210 twenty-noded isoparametric elements with a total of 6033 nodes arranged as shown in Figure 2. Nodes along the vertical boundaries may translate freely along the boundaries but are fixed against displacements normal to these boundaries. The nodes at the base are fixed against displacements in both directions.

In describing the results of 3D analysis, two stability criteria are presented as suggested by Lo *et al.* [2]; the first is the displacement around the tunnel opening that may be considered to indicate ground instability if excessive displacement developed. The second stability criterion related to the development of plastic zones around the advancing face. For stable tunnels, plastic zones only develop at the face corners whereas for unstable ground a continuous plastic zone is formed at and in front of the tunnel face.

In order to investigate the effects of the rock mass strength on tunnel stability and deformation, the strength was reduced gradually by reducing the cohesion (c). Five cases were examined representing a range of rock mass quality from good to poor quality rock mass using c = 9, 4.5, 3.5, 2.5 and 1.2 MPa. These values correspond to a ratio of rock mass strength to in situ stress (σ_{cm}/p_o) of about 3.0, 1.4, 1.0, 0.8 and 0.4 respectively. The in situ stress is represented by the average principal stress defined as $p_o = (\sigma_v + \sigma_h) / 2$, where σ_v and σ_h are the vertical and horizontal stresses respectively.

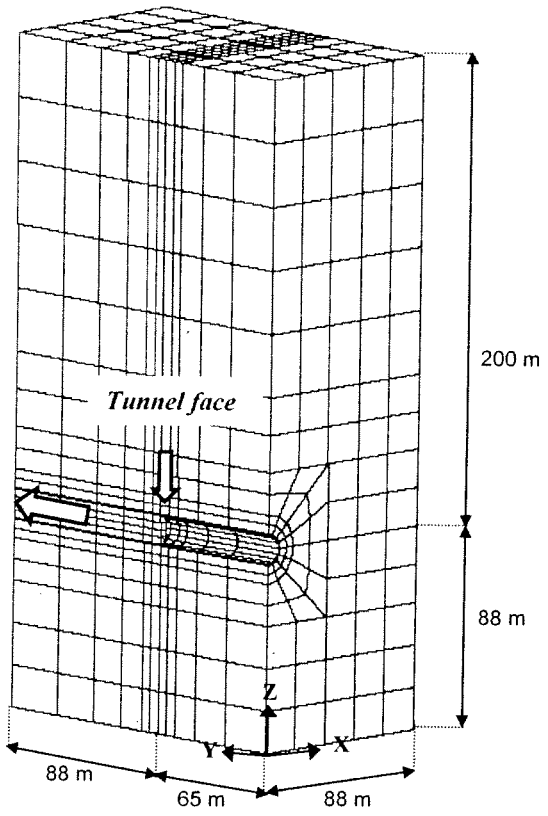

Figure 2. Finite element mesh used in the 3D analysis

5. TANGENTIAL STRESSES

The results of analyses give a complete description of stresses, displacements and plastic zones around the tunnel. For space limitations, only some results of stresses and plastic zones can be presented in this paper.

The advancement of a tunnel face in a stressed rock mass results in the disturbance and redistribution of the primary in situ stress field. This disturbance involves both changes in magnitude and orientation of stresses in the proximity of the tunnel boundary. The tangential stress distribution at a plane strain cross section as well as the changes in tangential stresses with distance from the tunnel face is presented in the following sections.

5.1 Tangential stresses at a plane strain cross section and the tunnel face
The distribution of tangential stresses at a plane strain cross-section across the tunnel is shown in

Figure 3. Compressive stresses were calculated at the tunnel crown and invert for the entire range of rock mass strengths examined. These stresses decreased from 52 MPa for (σ_{cm}/p_o) = 3.0 to about 25 MPa for (σ_{cm}/p_o) = 0.4. Tensile stresses were observed at the springline for the range (σ_{cm}/p_o) of 3 to 1. As the strength decreased, compressive stresses started to develop and reached a value of about 5.6 MPa for (σ_{cm}/p_o) = 0.4. The calculated tangential stresses for the elastic case were compared with the closed form solution from which maximum stresses of about 58 MPa and –5 MPa were found at the tunnel crown and springline respectively. These values are slightly higher than the calculated values using the finite element analysis. This may be attributed to the fact that stresses are being calculated in the finite element analysis at the Gauss points, which are located at a distance of about 0.5 m from the tunnel perimeter for the elements surrounding the tunnel opening.

The significance of the previous results is that, under a given high in situ stress value, the rock mass strength has a great influence on the redistributed tangential stresses around the tunnel opening. A failure pattern in the form of cracking along the springline may develop due to the possible development of tensile stresses in the rock, for unlined tunnels in strong rock. It should be noted that high tensile stresses induced at the springline level have been measured by Lo *et al.* (1984) in strong rock (σ_{cm}/p_o = 17) and are consistent with the theoretical results.

To investigate the effect of the stress redistribution on the tunnel face and to examine the possible overstressing of the rock mass at the face, tangential and radial stresses along the crown-invert diameter were calculated and shown in Figures 4 and 5 respectively. Tangential stresses are compressive near the tunnel crown and invert for the range of rock mass strength examined as shown in Figure 4. These stresses ranged between 2.5 to 3 times the average in situ stresses, p_o. In Figure 5, tensile stresses were found for high strength rock mass with a maximum value at the face center as shown in Figure 5a. These results are consistent with those reported by Lo *et al.* [1]. Under such conditions, tensile fracture occurs as a phenomenon of rock burst. Case histories reported by Martna [8] indicated that severe rock bursting conditions occurred in high strength rock during the excavation of a tunnel in Sweden. Rock bursting was manifested near the tunnel heading, following the face advance, and seldom at distance greater than 3a, where a is the tunnel radius, from the face.

As the strength decreased, compressive stresses started to develop at the edges near the crown and invert (see Figure 5). With further decrease in the strength, an almost uniform distribution of compressive stress was observed. It is well known that rock burst seldom occurs in weak rock. These results suggest that face stability may involve fundamentally different mechanism of failure in strong and weak rock.

A summary of results is given in Figure 6. It can be seen that similar behavior for the rock at the face center and springline, where tensile stresses started to develop at rock mass strengths of about 1 to 1.5 times the in situ stress and elastic response was found at (σ_{cm}/p_o) of about 2. These results are of practical importance for preliminary design assessment. In addition to controlling deformations, the temporary supporting system should be designed to resist the stress induced instability of the tunnel. The existence of stress concentration at the crown and invert may lead to roof fall and floor heave in weak rock masses or rock bursting in high strength rock masses.

5.2 The effect of face advance on the tangential stress distribution

In the previous section, the final stresses at the tunnel face and the stresses developed at a plane strain cross section were presented. During the face advance, however, stress magnitude and orientation keep changing until the plane strain conditions are reached. The effect of face advance on the tangential stress changes is discussed in this section.

Tangential stresses at several cross sections along the tunnel are plotted in Figures 7a and 7b for the crown and springline respectively. At the tunnel crown, tangential stresses close to the face are higher than at the plane strain cross-section for low quality rock mass, (σ_{cm}/p_o) = 0.4-1.0 with significant stress increase of about 100% for (σ_{cm}/p_o) = 0.4 at a distance of 5 m from the face. As the rock mass strength increased, a more uniform stress distribution was found along the tunnel. The practical significance of this observation is that the stress redistribution near the face due to tunnel excavation depends on the ratio of the rock mass strength to in situ stress. Higher

tangential stress concentrations occur near the face for the relatively poor quality rock mass. Therefore, excavation in poor quality rocks should proceed with caution and temporary lining should be installed as close to the face as possible to avoid local instability at the tunnel crown.

At the tunnel springline, a similar but less pronounced trend was found for low quality rock where the tangential stresses (compressive) increased near the face. For (σ_{cm}/p_o) greater than 1.0, tensile stresses developed along the tunnel with a significant increase of about 100% for (σ_{cm}/p_o) = 3.0 as shown in Figure 7a. The implication of this finding is obvious. Although stress levels developed at the springline are small compared to in situ stresses, tensile stresses can rapidly develop close to the face which may lead to local instability and cracking along the springline if tensile stresses exceeded the tensile strength of the rock.

6. PLASTIC ZONE DEVELOPMENT

In order to simplify the identification and 3D plotting of plastic zones, elements with several (more than 9) plastic Gauss points are considered to become plastic and are plotted in Figures 8a and 8b. Using this method, the extent of the plastic zone is approximated to a distance of half an element width. To illustrate the extent of the plastic zone at the tunnel crown and haunches (at 45°), two cross sections were considered as shown in Figures 8a and 8b respectively.

For the cases of (σ_{cm}/p_o) = 1.4, the plastic zone was uniformly distributed around the tunnel circumference near the tunnel haunches. The radius of the plastic zone based on these results was about 4 m from the tunnel. For (σ_{cm}/p_o) = 1.0 the distribution of the plastic zone was not uniform, such that, plasticity concentrated at the tunnel haunches with a radius of about 8 m from the tunnel circumference and 4 m elsewhere. Local plasticity at the tunnel face near the crown and invert was observed. As the rock mass strength decreased the plastic zone developed around the tunnel opening followed the same pattern discussed. However, the radius of plastic zone extended further at the tunnel haunches to a distance of about 16 m (see Figure 8b) from the tunnel circumference and increased to 8 m at the crown (see Figure 8a). A continuous plastic zone developed at the tunnel face with further strength decrease.

It is evident, from the previous results that the size of plastic zone around the tunnel opening shows a dramatic increase and a continuous plastic zone formed at the face when the uniaxial compressive strength of the rock mass was around about 0.4. Unless adequate support is provided, the tunnel may be unstable under such conditions.

7. SUMMARY AND CONCLUSIONS

The behavior of a large diameter tunnel in weak rock subjected to high horizontal stresses has been investigated. The analysis allows the computation of the complete stresses and deformation patterns as well as plastic zone development around the length of the tunnel and at the face.

Face stability involves fundamentally different mechanisms of failure in strong and weak rock. For the case of weak rock, stress concentration may lead to overstressing of the rock mass at the face causing local instability and possibly failure. Strong rock may experience a different failure mechanism where tensile stresses may occur at the face causing tensile fracture as a phenomenon of rock bursting.

Plastic zones concentrate at the tunnel haunches and extend along the excavated part of the tunnel up to a distance of about one tunnel diameter from the tunnel face. Adequate support at the face and springline is required when the ratio between rock mass strength to in situ stress falls below 0.4 at which a continuous plastic zone is formed.

8. ACKNOWLEDGEMENTS

This research is supported by the Natural Sciences and Engineering Research Council of Canada (NSERC) and an Ontario Government Scholarship in Science and Technology (OGSST).

9. REFERENCES

1. Lo, K.Y., Lukajic, B. and Ogawa, T. 1984. Interpretation of Stress-Displacement Measurements. Proceedings of Session Sponsored by Geotechnical Engineering Division, ASCE – GEOTECH 84. Atlanta, GA, pp. 128- 155.

2. Lo, K.Y., Ogawa, T., Sekiguchi, K. and Rowe, R.K. 1992. Large deformation and face instability in tunneling through thick fault zones. Canadian Tunneling Journal, pp. 77- 96.

3. Yuen, M.K., Erzinclioglu, A., Huang H.S. and Somerville, N. 1992. Design of diversion tunnels Niagara River hydraulic development. 45th Canadian Geotechnical Conference, Toronto.

4. Smith I.M. and Griffiths D.V. 1998. Programming the finite element method. third edition. John Wiley, London.

5. Abdel Meguid, M. 2002. Selected 3D aspects of tunneling. Ph.D. thesis, Civil Engineering Department, The University of Western Ontario. (In preparation).

6. Brown, P. T. and Booker, J. R. 1985. Finite element analysis of excavations. Computers and Geotechnics, Vol. 1, No. 3, pp. 207-220.

7. GID, version 6.0, 1999. International Centre for Numerical Methods in Engineering, Spain.

8. Martna, J. 1970. Rock bursting in the Sourva-Vietas Headrace tunnel. First Int. congress of the Int. Assoc. of Eng. Geology, Vol. 2, pp. 1134-1139.

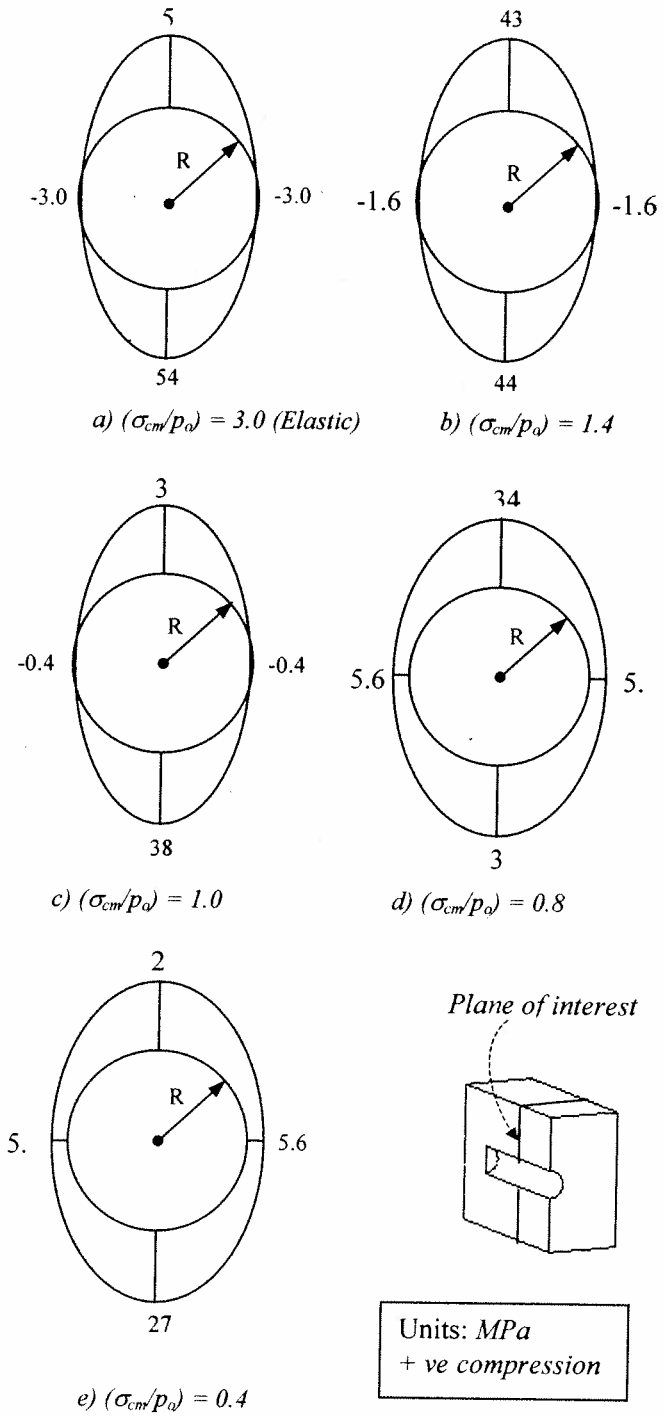

Figure 3. Distribution of tangential stresses at a plane strain cross-section of the tunnel

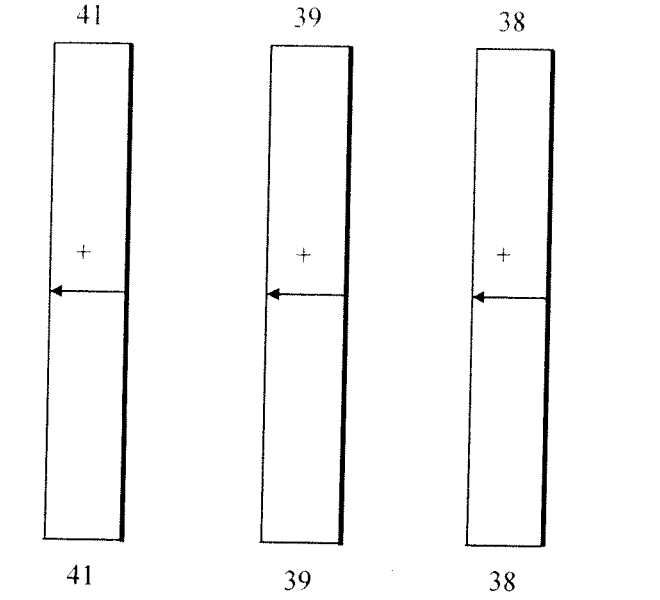

a) $(\sigma_{cm}/p_o) = 3.0$ b) $(\sigma_{cm}/p_o) = 1.4$ c) $(\sigma_{cm}/p_o) = 1.0$

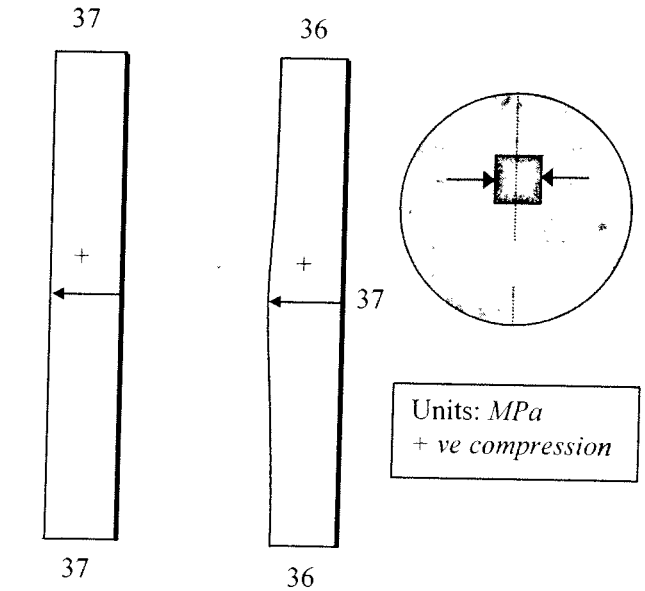

d) $(\sigma_{cm}/p_o) = 0.8$ e) $(\sigma_{cm}/p_o) = 0.4$

Figure 4. Distribution of tangential stresses at the tunnel face

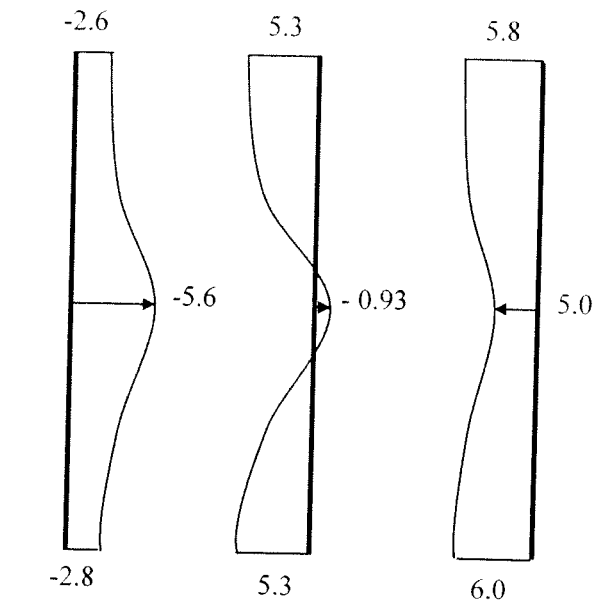

a) $(\sigma_{cm}/p_o) = 3$ b) $(\sigma_{cm}/p_o) = 1.4$ c) $(\sigma_{cm}/p_o) = 1.0$

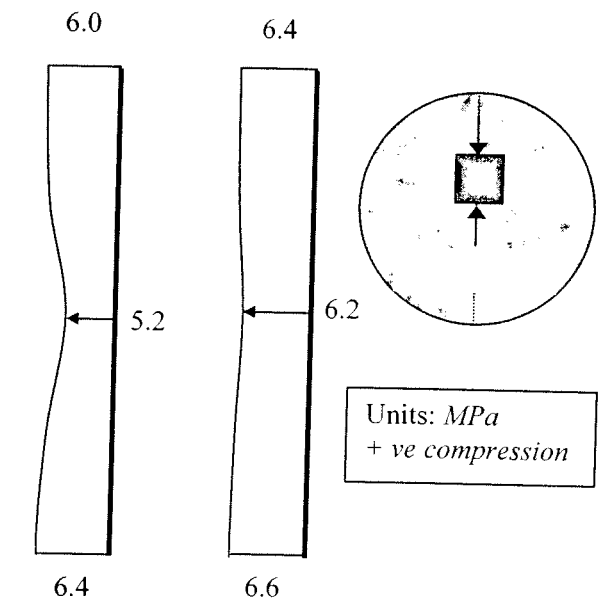

d) $(\sigma_{cm}/p_o) = 0.8$ b) $(\sigma_{cm}/p_o) = 0.4$

Figure 5. Distribution of radial stresses at the tunnel face

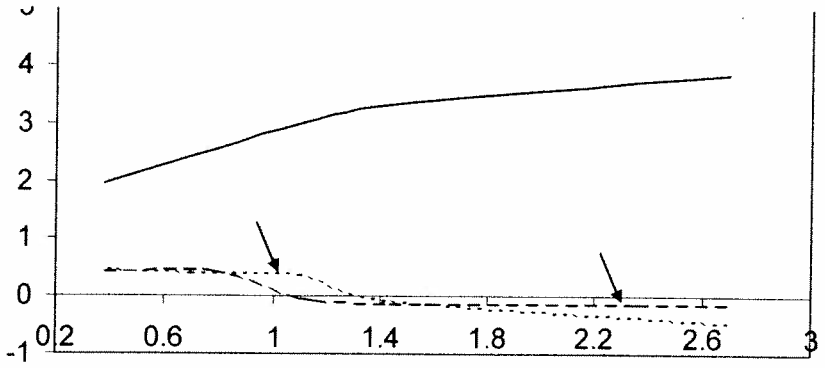

Figure 6. Relationship between rock mass strength and tangential stresses

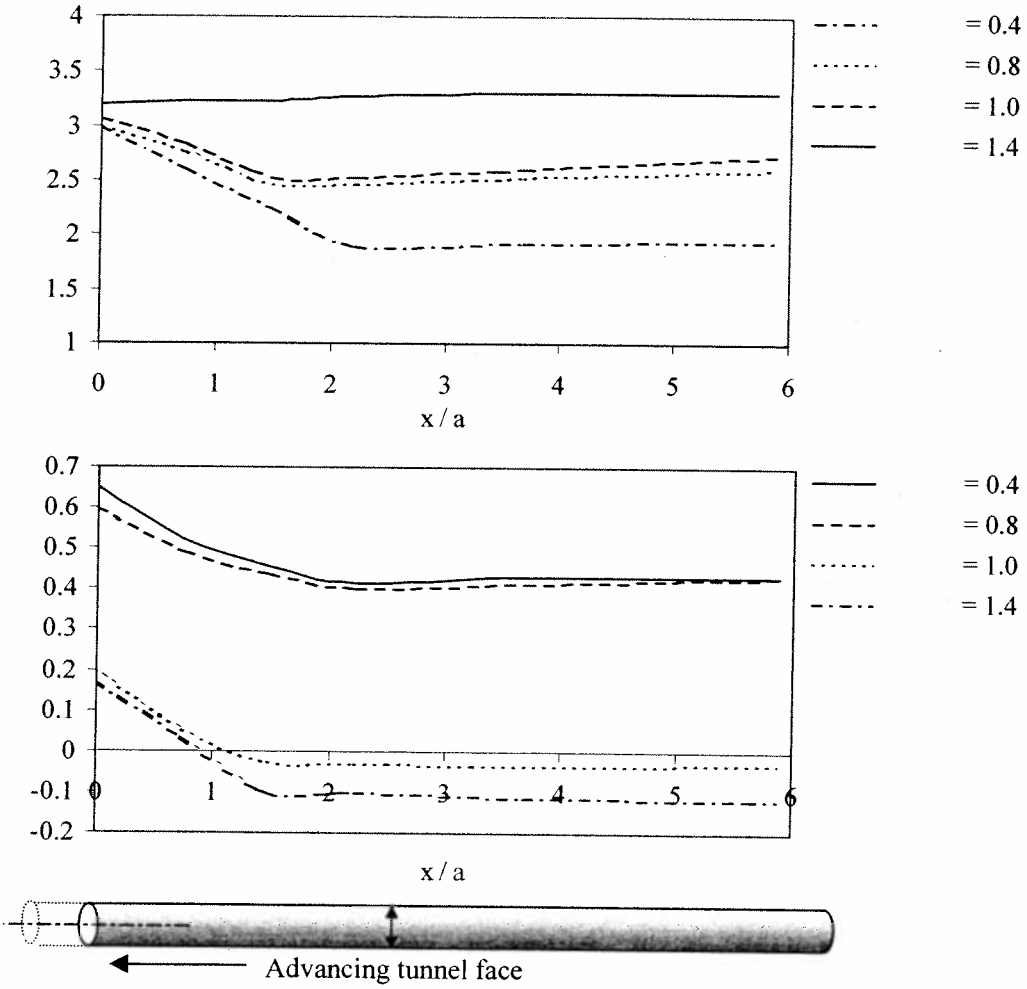

Figure 7. Variation of tangential stresses with distance from the tunnel face

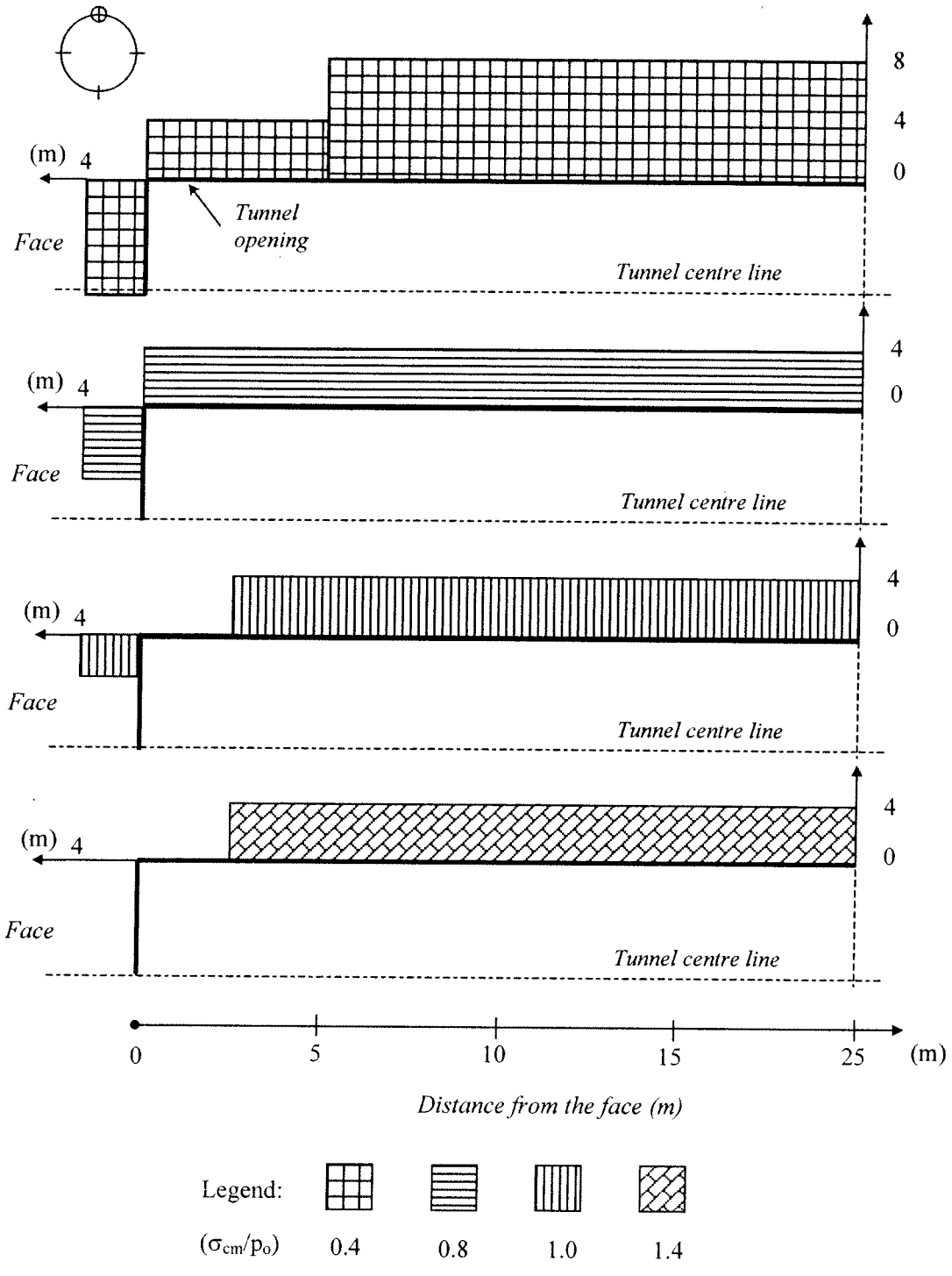

Figure 8(a) Approximate extent of plastic zone at the tunnel face and crown

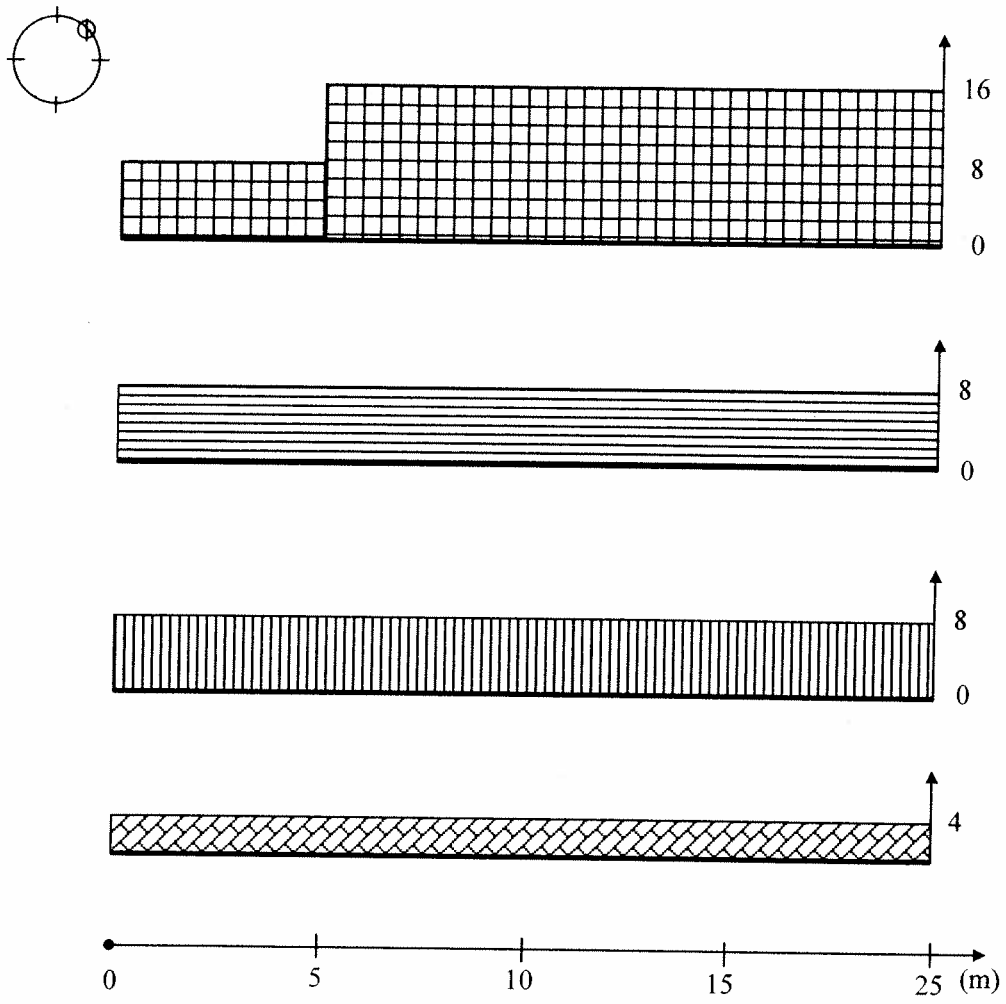

Figure 8(b) Approximate extent of plastic zone at the haunches